End-Bridging Monte Carlo Simulation of Bulk and Grafted Amorphous Polyethylene Above and Below the Glass Transition

Orestis Alexiadis,[†] Vlasis G. Mavrantzas,[†] Rajesh Khare,[‡] Job Beckers,[§] and Arlette R. C. Baljon*[,§]

Department of Chemical Engineering and Institute of Chemical Engineering and High Temperature Chemical Processes (FORTH -ICE/HT),University of Patras, GR 26504, Patras, Greece, Department of Chemical Engineering, Texas Tech University, Box 43121, Lubbock, Texas 79409-3121, and Department of Physics, San Diego State University, San Diego, California

Received May 24, 2007; Revised Manuscript Received November 20, 2007

ABSTRACT: The very efficient end-bridging Monte Carlo (EBMC) method has been employed in order to simulate an amorphous, polydisperse 80-chain large C_{156} polyethylene (PE) system in atomistic detail over a wide range of temperatures (from 600 down to 150 K) and determine its glass transition temperature (T_g). Two sets of simulations have been performed: one with a bulk, isotropic sample and the other with a thin film in which all the 80 PE chains were grafted on a hard substrate on one side (corresponding to a high grafting density equal to $\sigma = 1.75$ nm^{-2}) and exposed to vacuum on the other side. In the simulations, a united-atom model was employed for PE ensuring that only the purely amorphous phase of PE was simulated at all temperatures. In all cases, very long simulations were carried out in order to give enough time for the system to relax at all length scales. For all temperatures studied, the longest relaxation time was found to be present by descriptors associated with the system's long-range conformational characteristics. In contrast, more local, internal structural features were always faster in equilibrating. As a result, the time autocorrelation function for the chain end-to-end unit vector, $f_{\mathbf{u}}(t)$, was found to drop to zero and then clearly fluctuate around this value only for temperatures higher than about 220 K for both systems. For lower temperatures, $f_{\mathbf{u}}(t)$ did not relax completely, even after 2×10^7 CPU seconds. Additional volumetric simulation data demonstrated a sharp change in the density and potential energy of both systems in the neighborhood of the 230 K, which are considered as features of the glass transition for amorphous PE. The T_g value suggested by the present EBMC simulations for amorphous (bulk or grafted) PE is (230 ± 10) K, which is consistent with the value of 237 K measured experimentally by Wunderlich [*J. of Chem. Phys.* **1962**, *37*, 1203] and Loufakis and Wunderlich [*J. Phys. Chem.* **1988**, *92*, 4205] for PE in the limit of zero crystallinity. Further, the predicted change in the heat capacity at constant pressure at the glass transition is $\Delta c_p = 1.2 \times 10^{-4}$ kcal g^{-1} K^{-1}, which is very close to the value of 1.5×10^{-4} kcal g^{-1} K^{-1} measured experimentally by Wunderlich [*J. of Chem. Phys.* **1962**, *37*, 1203]. Additional results on the temperature dependence of the conformational and structural properties in the two PE systems are also reported and discussed in detail.

1. Introduction

The glass transition temperature (T_g) is one of the most important characteristics of amorphous polymeric materials that governs their usage for practical applications; the T_g of bulk polymers has thus been the subject of research studies for many decades. In recent years, applications such as those in the microelectronics industry have renewed the interest in the T_g and its effect on the thermomechanical properties of polymer thin films. In this work, we investigate the applicability of a newly developed Monte Carlo (MC) simulation technique for using a chemically realistic united-atom model of the polymer chains to model the T_g behavior of both the bulk and the thin films of amorphous polyethylene.

The effects of nanoscale confinement (including ultrathin films) on the T_g of polymers have been presented in a recent comprehensive review.[1] This review shows that depending on the specific physics and chemistry of the system under study all three types of behavior can be observed: The T_g of the thin films can increase, remain the same, or decrease when compared to the T_g of the bulk. As an example, for the same polymer, polystyrene, the following observations have been reported in the literature: The T_g of freely standing polystyrene films is significantly lower (by 60 K or more) than the bulk T_g,[2−4] the T_g of polystyrene films supported on SiO_x is slightly lower (<10 K) than the bulk T_g,[4] while the T_g of polystyrene films supported on hydrogen terminated Silicon substrates is significantly higher (>60 K) than the bulk T_g.[5] These results clearly demonstrate the importance of accounting for the detailed chemistry of the polymer surface interactions for accurately capturing the effect of the surface on the T_g of the polymer film. Furthermore, the interfacial glass transition,[6] the structural relaxation in thin films of glassy polymers,[7] and the effects of polymer chain grafting on the T_g of polymer thin films[8,9] have also been studied experimentally. A detailed, molecular level representation of polymer behavior is required for explaining the multitude of the physical phenomena captured by these experimental studies.

Molecular simulations offer a unique vehicle for a direct investigation of the microscopic mechanisms underlying the glass transition behavior of complex materials such as polymers. A large number of such simulation studies of the polymer glass transition have utilized the bead-spring representation of chains, and a comprehensive review has recently appeared.[10] While the bead-spring models provide a detailed description of the physics of the glass transition phenomenon, investigation of the specific chemical effects necessitates the usage of either all-atom or the so-called united-atom models of polymer chains. MD simula-

* To whom correspondence should be addressed. E-mail: abaljon@mail.sdsu.edu.
[†] University of Patras.
[‡] Texas Tech University.
[§] San Diego State University.

10.1021/ma071173c CCC: $40.75
Published on Web 01/04/2008

tions have indeed utilized such chemically more realistic united-atom models to investigate the bulk glass transition behavior of polyethylene[11,12] and a number of other polymers.[13] The sizes of the systems investigated in these early studies as well as the simulation run lengths were small compared with the current standards. Nevertheless, these studies showed that the bulk T_g values obtained from the volume−temperature behavior were at the most 15−20 K higher than the experimental values of the bulk samples.[13] The glass transition behavior of polymer thin films has also been investigated via molecular dynamics (MD) simulations using the bead-spring models of polymer chains. Varnik et al.[14] studied the dynamics of short bead-spring model polymer chains that are confined between repulsive walls and noted that a reduction in the film thickness leads to a decrease in the critical temperature of the mode-coupling theory. Similarly, an MD study of bead-spring polymer chains in free-standing films as well as films supported on a weakly attractive surface also showed a decrease in the film T_g compared to the bulk T_g.[15] MD studies[16]and experiments[9] of films grafted to attractive surfaces showed an increase in the glass transition temperature.

Although MC simulations do not directly capture the dynamics, in principle, they are expected to provide a better sampling of the phase space available to the system, which becomes an important consideration as the system temperature approaches the T_g. Most of the MC simulation studies of glass transition that have been reported in the literature have utilized an ideal coarse-grained model of the polymer chains. The MC simulations of supercooled polymeric systems carried out using the bond fluctuation lattice model have been summarized in two reviews.[17,18] The T_g was determined in these lattice MC simulations from the temperature dependence of either the energetic and structural properties[19] or the relaxation time[18] of the polymeric system. More recently, MC simulations have also been used to investigate the glass transition behavior of free-standing polymer films.[20] In that work, for polymer chains modeled on a lattice, simple configurational bias MC moves were supplemented by nonlocal rebridging moves to achieve an efficient sampling of the phase space of the glass forming system.

The effectiveness of the specific MC moves used is an important consideration in judging the ability of the MC simulations for efficient sampling of the phase space. The sampling capability of the MC moves plays an even bigger role when chemically realistic all-atom, or united-atom models of polymer chains are used in the simulations. To this end, a few novel MC moves have been proposed in recent literature for the simulation of polymeric systems. One of these moves, the end-bridging move, has been shown to lead to a large acceleration in the sampling of the phase space for systems such as polyethylene, polyisoprene and polybutadiene melts,[21−24] polymers grafted on substrates,[25−27] oriented systems,[28,29] branched polymers,[30] etc. providing excellent predictions of their volumetric, conformational, and structural properties. It is this move, end-bridging Monte Carlo, that will be used in the current work.

In summary, previous simulation work for polymer thin films has mainly utilized the coarse-grained models of polymers. Such models provide a detailed description of the physics of the glass transition phenomenon. Our long-term interest, however, lies in the investigation of the effects of the specific chemical interactions on the glass transition process. The objectives of this work are thus two-fold. First, we are interested in exploring the applicability of the recently proposed EBMC simulation technique to determine the glass transition temperature of bulk and thin films of polymers. In this initial MC study of polymer thin films, the solid substrate is represented using a "hard" surface and thus the surface effects are captured only via the excluded volume interactions. Second, we are interested in assessing the ability of this simulation technique to efficiently sample phase space when a chemically realistic united-atom model of the polymer chains is used. The rest of the paper is organized as follows. We begin with a description of the chain model used and give the details of the MC simulation moves, including the end-bridging move. We then describe the results for the glass transition temperature of the bulk and the grafted thin films of the model polyethylene system. We conclude with a summary of our results.

Table 1. Atomistic Molecular Model Used in the EBMC Simulations: Potential Functions and Parametes

type of interaction	potential function and parameters
nonbonded interactions	$U_{LJ}(r) = 4\epsilon_{LJ}[(\sigma_{LJ}/r)^{12} - (\sigma_{LJ}/r)^6]$ $\epsilon_{LJ} = 0.0914$ kcal mol^{-1}, $\sigma_{LJ} = 3.95$ Å
bond lengths	constant, $l = 1.54$ Å
bond bending angles	$U_{bend}(\theta) = 1/2k_\theta(\theta - \theta_0)^2$ $k_\theta = 124.188$ kcal mol^{-1} rad^{-2}, $\theta_0 = 114°$
dihedral angles	$U_{tor}(\phi) = \sum_{i=0}^{8} \alpha_i \cos^i(\phi)$ $a_0 = 1.99$, $a_1 = 4.23$, $a_2 = -0.6$, $a_3 = -7.17$, $a_4 = 4.5$, $a_5 = 3.9$, $a_6 = -8.92$, $a_7 = -3.45$, $a_8 = 5.6$ (kcal mol^{-1})

2. Systems Studied, Molecular Model, and Simulation Method

Two sets of simulations have been performed in this work: one with an isotropic bulk polyethylene system and the other with a thin polyethylene film consisting of grafted chains on a hard substrate on the one side (e.g., at the bottom) and exposed to vacuum on the other side (e.g., at the top) along the z direction of an xyz Cartesian coordinate system (z denotes the direction perpendicular to the solid boundary). Both sets of simulations have been carried out with 80 chains of polyethylene in the simulation box with mean chain length $X = 156$ (we call this a C_{156} system). The chain length distribution in both cases was a uniform distribution in the closed interval $[X(1 - \psi), X(1 + \psi)]$, where ψ denotes the half-width of the chain length distribution reduced by the number average chain length X. In all simulations, a value of $\psi = 0.9$ was used, corresponding to a polydispersity index I of 1.27. The bulk simulations were carried out in a cubic box and periodic conditions were applied along all three directions x, y, and z of the Cartesian coordinate system. The thin film simulations were carried out in an orthorhombic box with different edge lengths, L_x, L_y, and L_z, along the x, y, and z directions of the coordinate system. In this case, periodic boundary conditions were applied only along x and y, meaning that an infinite system is considered there; in contrast, a finite film thickness was assumed in the z direction equal to the width of the simulated film. The dimensions L_x and L_y of the orthorhombic box in the x and y directions were kept constant, both equal to 67.6 Å, meaning that the grafted system was simulated under conditions of constant and rather high grafting density, $\sigma = 1.75$ nm^{-2}.

The molecular model used in the two sets of simulations is identical to that employed in our previous simulations of polyethylene (PE). It is a united-atom model, in which each methyl and methylene group along the chain is regarded as a single interacting site. Bond lengths are kept constant, equal to 1.54 Å, flexible bond angles are sampled according to van der Ploeg and Berendsen potential,[31] torsion angles are governed by the Toxvaerd potential,[32] while for all intramolecular interactions between segments separated by more than three bonds along the chain and for all intermolecular interactions methylene groups are treated as united Lennard-Jones (LJ) force centers with a collision diameter equal to 3.95 Å and a well depth equal to 0.0914 kcal mol^{-1}.[33] The cutoff distance of the LJ potential was set equal to 9.1 Å. Table 1 summarizes the functional form of the interactions considered in the model and

the values of the parameters entering the expressions for the various potential functions.

The bulk simulations were executed with the EBMC method presented in the literature[21,22] with an initial configuration for the 80-chain C_{156} PE system generated by the three-stage constant density energy minimization technique of Theodorou and Suter.[34] The EBMC simulations were conducted in the $\{N_{ch}nTP\mu^*\}$ semigrand canonical ensemble,[21] where the following variables are kept constant: the pressure P, the temperature T, the total number of chains N_{ch}, the total number of mers n, and the spectrum of the relative chemical potentials μ^* of all chain species except for two (the reference species) in the system. The MC moves employed were reptations, end rotations, flips, concerted rotations, configurational biases, end-bridgings, and volume fluctuations in the ratio (% of attempted moves) 5:5:5:32:10:42:1, respectively. With this mix of moves, a number of simulations were carried out at a pressure P of 1 atm and temperatures T ranging from 600 K down to 150 K.

The simulations with the grafted system were carried out by employing the modified EBMC method presented in the literature,[25−27] where certain chain connectivity combinations that result in chains grafted to the substrate by both ends or not grafted at all are disallowed. The statistical ensemble in which these simulations are realized is the $\{N_{ch}nL_xL_yTP\mu^*\}$ ensemble (meaning that the simulations are performed at a fixed grafting density σ) but with the spectrum of chemical potentials suitably tuned (through an iterative analytical−numerical procedure) so that a strictly uniform distribution of chain lengths is eventually reproduced.[27] The following mix of moves was employed in these simulations: 7% surface rotations, 3% end rotations, 10% flips, 15% generalized reptations, 10% configurational biases, 25% concerted rotations, and 30% end bridgings. With this mix of moves, a number of simulations were carried out at a pressure P of 0 atm (the simulated thin PE film is exposed to vacuum on its upper face) and temperatures T ranging also from 600 K down to 150 K.

To take advantage of the faster system equilibration at the higher temperatures, in both sets of simulations, a MC run at a lower temperature was always started from an equilibrated configuration obtained at the end of the simulation with the EBMC algorithm at a higher temperature. Through this, we were able to exhaustively simulate the two systems in a reasonable amount of computation time even at the lowest temperatures considered in this work (near or below their T_g). The results of the simulations, which eventually allowed for a comparison of the glass transition behavior between the grafted and the bulk systems, are described below.

3. Results

A. Computational Efficiency. The rate of evolution of the time autocorrelation function $f_{\mathbf{u}}(t)$ for the end-to-end unit vector $\mathbf{u}$ of the chain (in millions of MC steps or, equivalently, in millions of CPU seconds on an Opteron 248 (2.2 GHz) machine) was used as a measure in assessing the sampling efficiency of the EBMC algorithm. To get rid of the limiting value of $f_{\mathbf{u}}(t)$ at infinite time for grafted chains (which can explore only half of the space in the z direction), for both systems studied here (bulk and grafted), $f_{\mathbf{u}}(t)$ was defined as (see ref 25)

$$f_{\mathbf{u}}(t) = \frac{\langle \mathbf{u}(t+t_0)\cdot\mathbf{u}(t_0)\rangle - \langle \mathbf{u}(t+t_0)\rangle\cdot\langle \mathbf{u}(t_0)\rangle}{\langle \mathbf{u}^2(t_0)\rangle - \langle \mathbf{u}(t_0)\rangle^2} \qquad (1)$$

producing values always in the interval [0, 1] and also allowing for negative numbers for $f_{\mathbf{u}}(t)$ due to fluctuations in statistics.

The dependence of $f_{\mathbf{u}}(t)$ on temperature is shown in Figure 1a−c. Figure 1a shows that $f_{\mathbf{u}}(t)$ decays rather rapidly to zero for the simulated bulk system at all temperatures above 200 K within modest computation time. However, as the temperature is decreased below this temperature, the rate of equilibration slows down considerably, implying that the performance of the end-bridging move is significantly impacted by lowering the temperature. This happens because, as the temperature is decreased, (a) the acceptance rate of the move drops down and (b) a number of successive end-bridging moves tend to annihilate each other since they happen to perform in the reverse

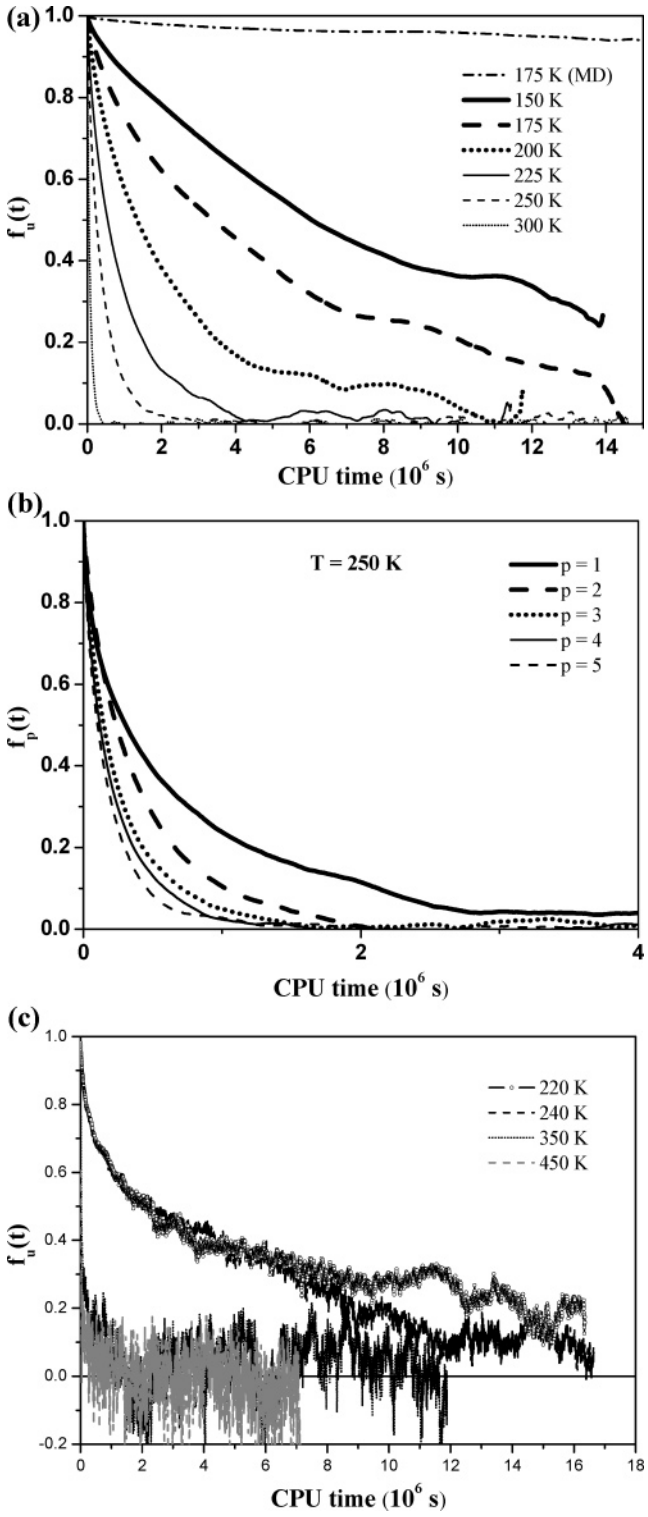

Figure 1. (a) Decay of the autocorrelation function of the chain end-to-end unit vector, $f_{\mathbf{u}}(t)$, with CPU time as a function of temperature for the bulk system. Also shown for comparison (uppermost curve) is the result for $f_{\mathbf{u}}(t)$ obtained at $T = 175$K with the parallel NPT MD method executed on a cluster of eight Intel Xeon nodes at 2.8 GHz. (b) Decay of the autocorrelation function $f_p(t)$ for the first five Rouse modes with CPU time at $T = 250$K for the bulk system. (c) Decay of the autocorrelation function of the chain end-to-end unit vector, $f_{\mathbf{u}}(t)$, with CPU time as a function of temperature for the grafted system.

Table 2. Acceptance Rates of the MC Moves Used in the Simulations of the Two Systems as a Function of Temperature

C_{156} ($I = 1.27$) bulk	reptations (%)	rotations (%)	flips (%)	concerted rotations (%)	end-bridgings (%)	vol fluctuations (%)
150 K	0.3	6.2	64.8	2.3	4×10^{-4}	2.5
175 K	0.5	6.8	67.2	2.5	4×10^{-4}	2.5
200 K	0.6	7.4	69.2	2.7	8×10^{-4}	2.7
225 K	0.7	7.9	70.8	3	0.002	2.9
250 K	1.3	8.8	72.1	3.5	0.004	3
300 K	2.4	10.7	74.1	4.6	0.014	3.5
350 K	4.2	13.2	75.4	6.2	0.044	4.3
400 K	6.1	15.6	76.6	7.8	0.1	4.8
450 K	8.4	18.4	77.7	9.4	0.2	5.5
600 K	16.1	26.5	80.3	14.7	0.7	7.7

C_{156} ($I = 1.27$) grafted	CCBs (%)	rotations (%)	flips (%)	concerted rotations (%)	end-bridgings (%)
150 K	18.5	27	30.5	0.33	1.05×10^{-4}
180 K	18.6	27.7	33.3	0.4	3.1×10^{-4}
220 K	18.8	33.6	36.2	0.58	0.001
270 K	19	34.9	39.1	0.96	0.006
300 K	19.1	37.1	40.3	1.3	0.014
350 K	19.3	38.1	42.2	2	0.043
400 K	19.7	40.4	44.2	2.9	0.094
450 K	20.9	43.1	45.9	4	0.18
500 K	22.1	44.2	47.6	5.3	0.28
600 K	24.7	47	50.6	8.1	0.57

direction to the previously accepted end-bridging moves. But despite these considerations, the move is so powerful that $f_{\mathbf{u}}(t)$ drops eventually to a very small value (close to 0.30) even for the lowest temperature simulated here ($T = 150$K), as indicated in Figure 1a.

For comparison, also shown in Figure 1a (uppermost curve) is the corresponding time autocorrelation function obtained for the simulated system at $T = 175$K by the NPT MD method executed in parallel on an eight-node Linux cluster of dual Intel Xeon workstations at 2.8 GHz with 1GB memory. It is seen that the rate with which this $f_{\mathbf{u}}(t)$ curve drops to zero is practically zero; after about 1.5×10^7 CPU seconds, it has dropped to only 0.98 indicative of the complete absence of any signs for relaxation.

Figure 1a presents evidence that the EBMC algorithm ensures equilibration of the longer length scales of the simulated C_{156} polymer in its highly dense submelt state even at temperatures as low as 200 K. But the question arises as to whether more local length scales (corresponding to internal structural features) of the system are equilibrated with comparable efficiency or not. This issue has been addressed in ref 22, where descriptors of the internal structure of bulk PE chains were defined and their relaxation with CPU time was analyzed at $T = 450$K. Although the dependence of relaxation time on subchain size was found to be strongly nonlinear, it was always monotonic verifying that the longest relaxation times are presented by the longest subchains. A similar analysis was carried out here, where we probed the relaxation of the chain internal structure at very local scales by accumulating the average time autocorrelation functions of the Rouse normal coordinates or modes in the C_{156} PE system in the course of the EBMC simulations. For a polymer chain consisting of N monomers (or Kuhn segments) with coordinates $\mathbf{R}_i$, where $i = 1, 2, ..., N$, the Rouse normal coordinates or modes $\mathbf{X}_p$, where $p = 0, 1, 2, ..., N - 1$, are defined as

$$\mathbf{X}_p = \sum_{n=1}^{N} \Omega_{np} \mathbf{R}_{n-1}, \quad \Omega_{np} = \sqrt{\frac{2 - \delta_{p0}}{N}} \cos\left(\frac{(n - 1/2)p\pi}{N}\right) \quad (2)$$

Each $\mathbf{X}_p$ with $p > 0$ represents the dynamics of the chain which includes N/p segments; therefore, its time autocorrelation function $f_p(t) = \langle \mathbf{X}_p(t)\mathbf{X}_p(0)\rangle / \langle \mathbf{X}_p(0)^2\rangle$ is representative of the local conformational relaxation of an internal segment along the chain of length equal to N/p. We have accumulated the functions $f_p(t)$ for all modes p along a C_{156} PE chain (i.e., from $p = 1$ to about $p = 40$) as a function of temperature and have confirmed that, indeed, their relaxation time decreases monotonically (although nonlinearly) with p mode. In Figure 1b, for example, we show the results obtained for the relaxation of the first five modes at $T = 250$ K (similar plots are obtained for all other temperatures), verifying that as segments along the chain become shorter their rate of relaxation increases (in terms of the CPU time) with the EBMC algorithm.

When the chains are grafted on the solid substrate, the function $f_{\mathbf{u}}(t)$ decays to zero slower (compared to the bulk system) by a factor between 3 and 4 that depends on the temperature (compare panels a and c of Figure 1 at the same temperature). This happens because (see also ref 25) all end-bridging combinations that result either in free chains or in chains which are grafted on the substrate by both ends are disallowed. A second reason is the lower acceptance rate of the end-bridging move due to chain orientation in the direction perpendicular to the boundary (as a result of the high grafting density). For the grafted system, therefore, full decorrelation of the $f_{\mathbf{u}}(t)$ function is realized only (see Figure 1c) for temperatures which are higher than about 240 K. For temperatures below 240 K, $f_{\mathbf{u}}(t)$ does not drop to zero within the limits of the available computation time.

Table 2 presents results for the acceptance rates of the moves employed in the simulations with the two systems as a function of temperature. The acceptance rate of the end-bridging move is small (of the order of 0.7%) even at the highest temperature simulated ($T = 600$ K). This low rate decreases further as T is reduced, falling to approximately 4×10^{-4}% for the bulk system and to approximately 1.05×10^{-4}% for the grafted system at $T = 150$K. Despite this, however, the algorithm can still ensure equilibration of the long- and especially short-length scale characteristics of the two PE systems, in particular of the bulk

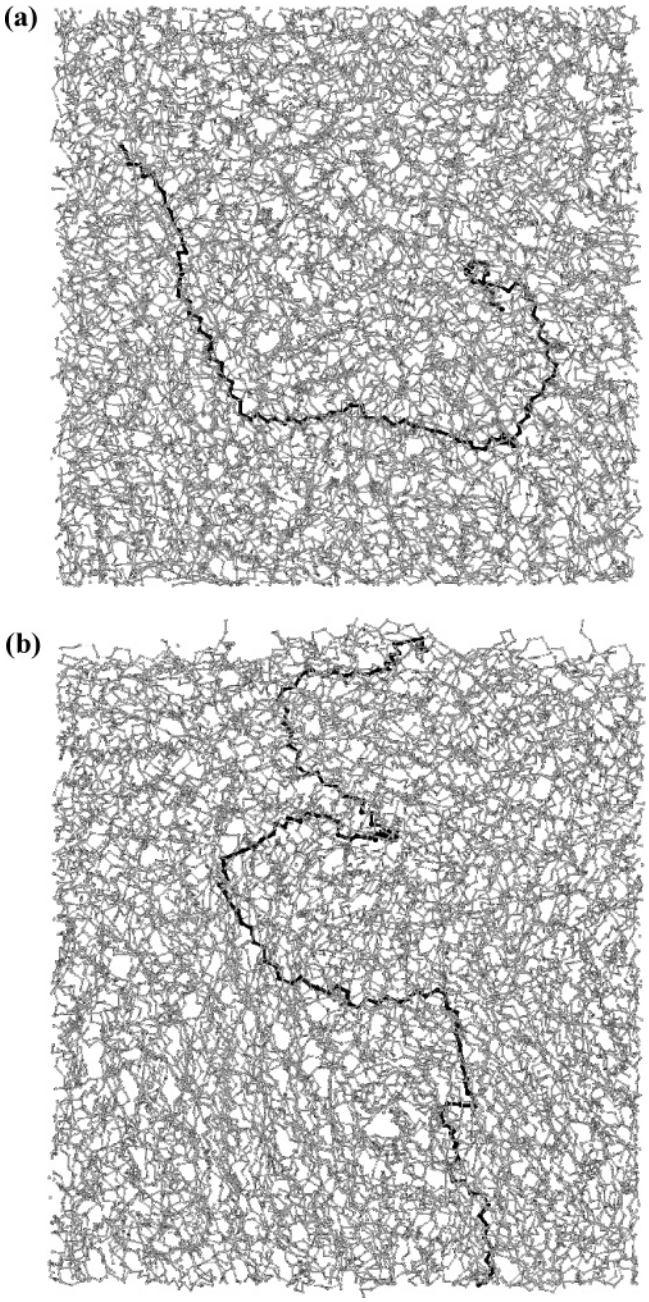

Figure 2. Typical atomistic snapshots of the bulk (a) and the grafted (b) systems at $T = 300$K at the end of the Monte Carlo simulation with the end-bridging algorithm.

one. The changes in chain connectivity and the jumps in the configuration space affected by an EBMC move are so drastic that, even if the success rate of the move is low and rather infrequent, they greatly enhance the rate with which molecular configurations are sampled. As a result, excellent equilibration of the thermodynamic and conformational properties of the two systems is observed not only in the melt state but also at significantly lower temperatures.

Typical snapshots of the two atomistic systems at the state of thermodynamic equilibrium at $T = 300$K are presented in Figure 2a,b, respectively.

B. Conformational Properties. Panels a and b of Figure 3 show the effect of temperature on the torsion angle (dihedral) distribution of the bulk and grafted C_{156} chain systems, respectively. At every temperature, perturbations in the distribution for the grafted system from the corresponding distribution

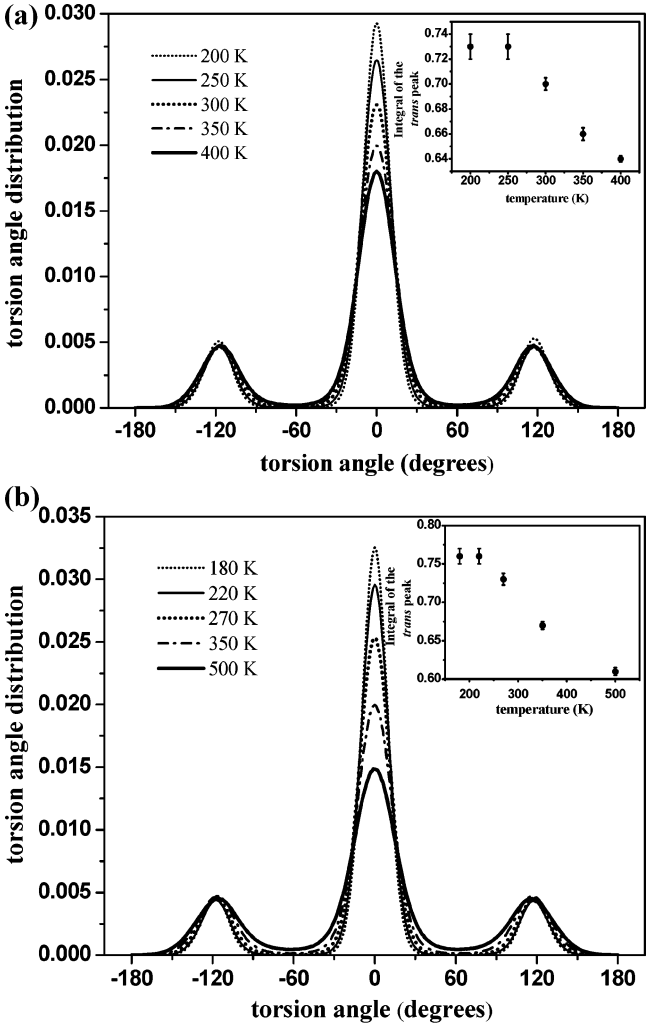

Figure 3. Variation of the dihedral angle distribution with temperature for the bulk (a) and the grafted (b) systems. In the insets, we show the variation with temperature of the integral of the trans peak in each system.

of the bulk isotropic sample (due to the presence of the two interfacial regions) are seen to be rather mild. As the temperature is lowered, a significant shift of angles from gauche to trans states is observed for both systems. To quantify this, the integral of the torsion angle distribution corresponding to the trans conformational states in Figure 3a,b (i.e., to torsion angles between $-60°$ and $+60°$) was calculated. The results (shown in the insets in the two figures) demonstrate an increase in the trans population from about 64% at $T = 400$ K (for both systems) to about 73% for the bulk and to about 76% for the grafted system at $T = 200$ K. With decreasing temperature, the chains are shown to unravel to intrinsically more elongated shapes.

For the bulk system, the increase in the trans population is accompanied by an increase in the value of the average squared chain end-to-end distance $\langle R^2 \rangle$ as demonstrated in Figure 4a. The simulation data of Figure 4a predict that $\partial \ln \langle R^2 \rangle / \partial T = -1.2 \times 10^{-3}$ K^{-1}; this prediction is in excellent agreement with experimental data reported by Ciferri et al.[35] for cross-linked polyethylene at 140 °C, according to which $\partial \ln \langle R^2 \rangle / \partial T = -1.1 \times 10^{-3}$ K^{-1}. We have also calculated the temperature dependence of the characteristic ratio or scaled intrachain segment length, $c_n = \langle R^2(n) \rangle / nl^2$, by accumulating the mean-square segment end-to-end distance $\langle R^2(n) \rangle$ along a chain as a function of the segment length n.[36,37] The results (see Figure 4b)

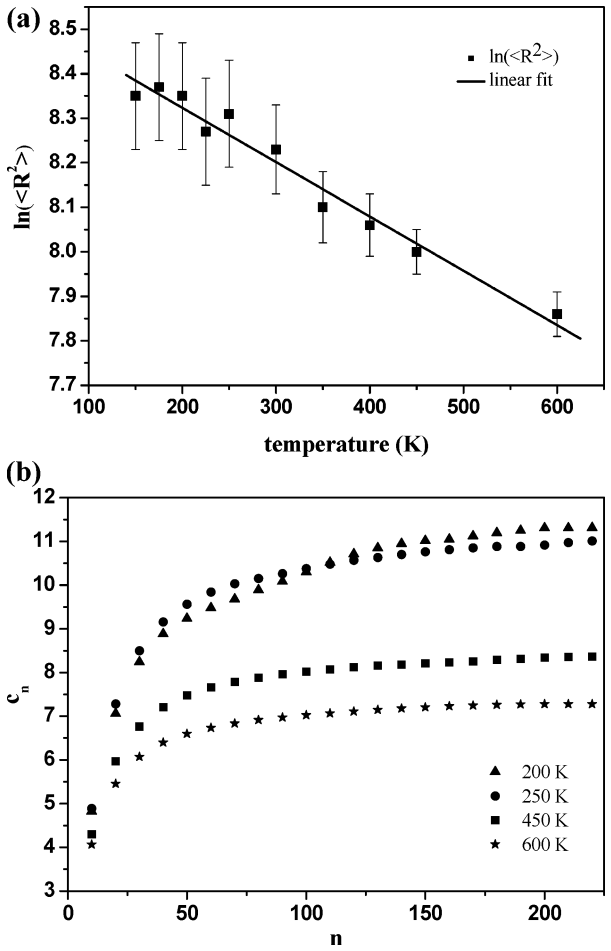

Figure 4. (a) Chain mean squared end-to-end distance, $\langle R^2 \rangle$, for the bulk C_{156} PE system and its variation with temperature. The straight line represents the best linear fit through the simulation data. (b) Scaled intrachain segment length, $c_n = \langle R^2(n) \rangle / nl^2$, vs segment length n and its variation with temperature.

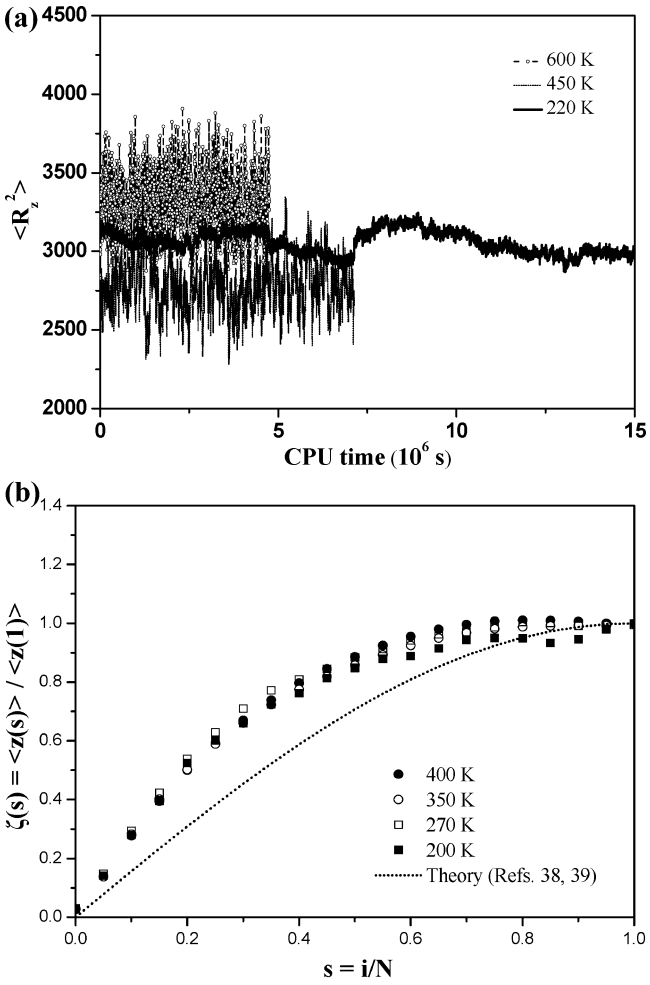

Figure 5. (a) Time evolution of the component of the chain mean-squared end-to-end vector perpendicular to the wall, $\langle R_z^2 \rangle$, for the grafted C_{156} PE system at three different temperatures. (b) Mean height of the backbone atom i above the substrate normalized with its maximum value, $\zeta(s) = \langle z(s) \rangle / \langle z(1) \rangle$, as a function of its normalized coordinate $s = i/N$ along the chain backbone, and its variation with temperature. The dashed line shows the analytical prediction of the Milner et al. theory (refs 38 and 39) for strictly monodisperse brushes, where $\zeta(s) = \sin(s\pi/2)$.

demonstrate the nonlinear increase of the characteristic ratio c_n with segment length n as well as the plateau value (characteristic ratio at infinite chain length, c_∞) at high enough chain lengths whose magnitude increases with decreasing temperature according to the law described above: $\partial \ln c_\infty / \partial T = -1.2 \times 10^{-3}$ K^{-1}.

For the grafted system, the relevant variables quantifying the effect of the confining boundary on the size of the chains are the three components $\langle R_x^2 \rangle$, $\langle R_y^2 \rangle$, and $\langle R_z^2 \rangle$ of the mean square chain end-to-end vector in the directions x, y, and z, respectively, of the coordinate system. Figure 5a presents the relaxation of $\langle R_z^2 \rangle$, i.e., of the component of $\langle R^2 \rangle$ in the direction perpendicular to the hard substrate, for three different temperatures: $T = 600$, 450, and 220 K. It is seen that (see also the collected data for all three components $\langle R_x^2 \rangle$, $\langle R_y^2 \rangle$, and $\langle R_z^2 \rangle$ as a function of T presented in Table 3; due to cylindrical symmetry $\langle R_x^2 \rangle = \langle R_y^2 \rangle$ and thus only the average value $\langle R_x^2 \rangle + \langle R_y^2 \rangle /2$ is shown in the Table) $\langle R_z^2 \rangle$ attains quite large values (compared to the isotropic $\langle R^2 \rangle /3$ result) indicative of the strong tendency of the grafted chains to get extended conformations in the direction perpendicular to the wall in order to avoid lateral overlaps. $\langle R_x^2 \rangle$ and $\langle R_y^2 \rangle$, on the other hand, attain values significantly smaller than the isotropic $\langle R^2 \rangle /3$ value indicative of a strong chain compression in the directions parallel to the wall.

An interesting point to notice in the data of Table 3 is that $\langle R_z^2 \rangle$ changes nonmonotonically with temperature; it decreases continuously as T is decreased from 600 to 300 K (followed by a slight increase in the values of $\langle R_x^2 \rangle$ and $\langle R_y^2 \rangle$), but then it increases as T is decreased even further, reaching eventually a constant value at around $T = 220$ K and below. This behavior is the result of two opposing factors: (a) the increase in the density of the system with decreasing temperature, which causes a decrease in the film thickness and thus also in the dimensions of the chains in the z direction (this is the only way by which the density can increase as the dimensions of the simulation box in the other two directions remain fixed in the course of the simulation with the grafted system) and (b) the tendency of the chains to open up and assume more extended conformations due to the increase in the population of the trans angles causing an increase in the overall chain dimensions. The net result is the observed nonmonotonic variation of the average chain dimensions in the direction perpendicular to the wall with temperature followed by a mild increase in the directions parallel to the wall.

Additional information about the conformational properties of the simulated grafted system is extracted by studying the average chain conformational path. Following previous work,[25] this quantity is defined as the average height $\langle z(i) \rangle$ of backbone atom i above the grafting surface, with $\langle z(i = 1) \rangle = 1.54$ Å (since the first atom of all chains is considered to remain fixed

Table 3. Average Chain Dimensions in the Directions Parallel and Perpendicular to the Hard Substrate as a Function of Temperature for the Grafted C_{156} PE System

T (K)	180	220	300	450	600
$\langle R_x^2\rangle + \langle R_y^2\rangle/2$	345 ± 20	335 ± 20	330 ± 20	305 ± 10	290 ± 10
$\langle R_z^2\rangle$	3050 ± 500	3050 ± 400	2450 ± 400	2770 ± 300	3300 ± 300

at a distance equal to one C−C bond length from the substrate). Due to different chain length species present in the simulations, the data are shown in terms not of the absolute atomic coordinate i along the chain but of the scaled coordinate $s = i/N$, where N is the molecular length of the chain to which segment i belongs. The resulting plots of the normalized mean height $\zeta(s) = \langle z(s)\rangle/\langle z(1)\rangle$ vs s and their temperature dependence are presented in Figure 5b. The figure shows that temperature has an infinitesimal effect on the mean conformational path of the grafted system (the four master curves in the figure for $T = 200$, 270, 350, and 400 K practically coincide), which qualitatively agrees with the predictions of self-consistent mean-field theories for grafted polymer brushes,[38,39] according to which, for strictly monodisperse systems and high enough grafting densities σ similar to the one studied here, $\zeta(s)$ should scale with s as $\zeta(s) = \sin(s\pi/2)$, i.e., independent of σ and T. This scaling has been derived on the assumption of the most probable conformational path (i.e., of the path that minimizes the system free energy) and is represented in Figure 5b by the dashed line. Of course, computed and analytically derived $\zeta(s)$ vs s curves are quantitatively different since they refer to totally different systems (see refs 25 and 26 for a more detailed discussion on this issue), but the overall conclusion is that they are only weakly (if not at all) dependent on temperature.

As mentioned above, with the specific parameter combination of the united-atom model employed in the present simulations and the application of the end-bridging move that destroys possible nuclei for crystallization and creates polydispersity, only the amorphous phase of PE is present in the simulated systems even for temperatures well below the melting point of the polymer. To verify that, indeed, no crystallization takes place in the course of the present EBMC simulations even when the temperature is decreased to very low values, we calculated the probability density function of all-trans sequences along a PE chain for the bulk systems as a function of the length of the trans sequence. The results obtained for several temperatures are shown in a log-linear plot in Figure 6. Despite the increase in the occurrence probability of longer all-trans sequences with decreasing temperature, practically straight lines are obtained in all cases verifying the complete absence of any tendency for the systematic development of crystalline regions.

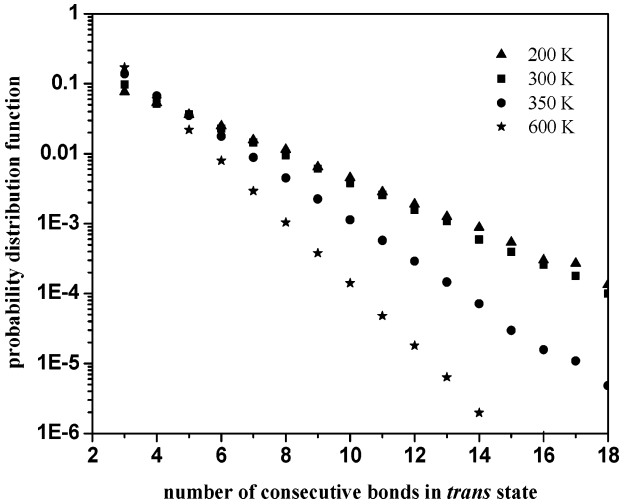

Figure 6. Log-linear plots of the probability density function of all-trans sequences along a C_{156} PE chain at various temperatures for the bulk system.

Further evidence for the purely amorphous structure of the two simulated systems is provided by the plots of the intermolecular pair distribution functions presented in parts a and b of Figure 7. Figure 7a shows plots of the segment intermolecular pair distribution function $g(r)$ for the isotropic bulk system at four different temperatures: $T = 450$ (i.e., well above the melting point of the simulated C_{156} PE system), 350 (just below its melting point), 300 and 150 K. Clearly, as the temperature is lowered, the peak corresponding to the first shell of intermolecular neighbors shifts to somewhat shorter distances; simultaneously, its height (and those of the shells at longer distances) is enhanced. These are manifestations of a denser atom−atom packing and, as a consequence, of an increase in the density of the system with decreasing T. However, no signals for polymer crystallization are detected. Figure 7b shows plots of the segment intermolecular pair distribution function $g_{xy}(r)$ for the grafted system in the directions (x−y) parallel to the solid substrate, at the same temperatures ($T = 450$, 350, 300, and 150K). These plots have been obtained by calculating the

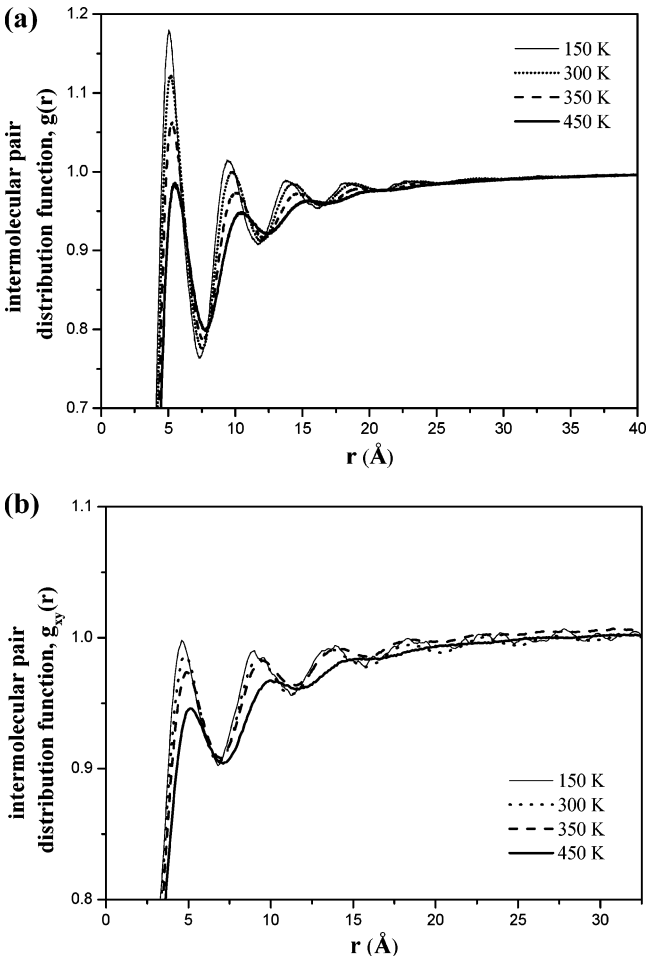

Figure 7. (a) Intermolecular pair−pair distribution function, $g(r)$, in the bulk system at various temperatures. (b) Intermolecular pair−pair distribution function parallel to the (x-y) solid substrate, $g_{xy}(r)$, in the grafted system at various temperatures.

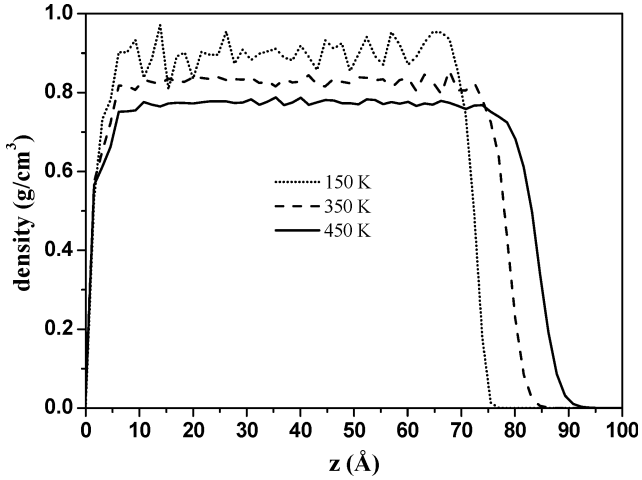

Figure 8. Local mass density profile in the grafted C_{156} PE system at several temperatures.

number of intermolecular neighbors in the space of a differential volume around a reference mer in the bulk region of the grafted melt (i.e., in the region between 10 and 60 Å from the grafted plane, see also Figure 8 below) between two concentric cylinders centered on the reference mer and with their axes perpendicular to the substrate. According to Figure 7b, a noticeable decrease of intermolecular neighbors is observed in the direction parallel to the substrate relative to the isotropic case at the same temperature, which is a direct manifestation of the induced chain orientation in the *z* direction.

The absence of local order in all three dimensions for the bulk system and along *x* and *y* directions for the grafted film was further confirmed by analyzing the average values of the second order (P_2) Legendre polynomials of the first kind for the unit vectors (chords) connecting the midpoints of successive skeletal C−C bonds. No signals of local ordering were detected except for the grafted film in the direction perpendicular to the wall.

C. Volumetric Properties. Figure 8 shows the variation of the local mass density ρ for the grafted system with distance *z* from the solid substrate at several temperatures. As discussed in detail in refs 25 and 26, the local mass density profile $\rho(z)$ exhibits two zones of reduced density at the two boundaries of the system: near the wall (which is of purely entropic origin) and at the polymer/vacuum interface (where one observes the characteristic sigmoidal shape typical of a polymer/vacuum interface). On the other hand, in the middle or bulk region of the system, ρ remains practically constant. This constant value depends on the temperature. For the simulated grafted C_{156} PE systems, this dependence is described in Figure 9 together with the EBMC simulation predictions for the density of the corresponding isotropic bulk C_{156} PE system. Error bars, represented as variance of the mean in each bin for the grafted system or as obtained by analyzing different blocks of the trajectory file, have also been included in the two plots. Within the statistical error, the two sets of data are identical; this indicates that, at every temperature, the two systems (the isotropic one and the bulk region of the grafted film) have the same density.

D. Determination of the T_g. The temperature variation of the density shown in Figure 9 can be used to estimate the glass transition temperature T_g of the two systems by fitting the data at low and high temperatures with straight lines. For both of them, the two lines coincide and cross at a point between 220 and 240 K. This common crossover point is an estimate for the

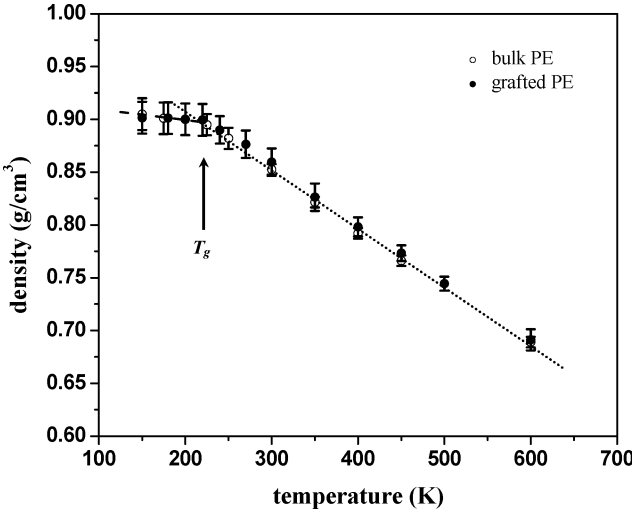

Figure 9. Effect of temperature *T* on the density of the bulk C_{156} PE system (open circles) and the density in the bulk zone of the grafted C_{156} PE system (filled circles).

glass transition temperature in the two systems.[16] Remarkably, this is the lowest temperature for which the employed EBMC algorithm could drive the autocorrelation function for the chain end-to-end unit vector to zero within reasonable CPU time.

Our estimated value for the T_g value of amorphous PE is very close to the value of 237 K reported by Wunderlich[40] and Loufakis−Wunderlich[41] for PE in the limit of zero crystallinity. This is very encouraging despite a number of factors that are different between the simulation and the experimental measurements. For example, the results reported by Wunderlich for the amorphous phase were obtained on semicrystalline PE samples by extrapolating to 0% crystallinity. Further, the system used in the EBMC simulations is characterized by a polydispersity index which is higher than that used in the experimental measurements.

As far as the thin grafted film is concerned, although, one would naively expect that the dynamical restrictions imposed by chain grafting would increase its glass transition temperature, the interaction with the surface has to be taken into account as well. In the case at hand, although the surface interaction is unfavorable, the fact that the grafted system is characterized by an extended bulk zone with density equal to that of the corresponding isotropic system results in a glass transition temperature practically the same as that of the bulk system.

A second estimate of T_g can be obtained by analyzing the temperature dependence of the *enthalpy*, *H*, in both systems. The enthalpy $H = U + PV$ is the sum of the total energy *U* of the system (the sum of the potential energy U_{pot} and the kinetic energy U_{kin}) and the *PV* term. For the grafted system, the pressure is equal to zero and hence the second term does not contribute (it is identically zero). For the bulk system at atmospheric pressure, this second term can also be neglected since its contribution is minimal. On the other hand, the kinetic energy, which is not available in the MC simulations, is in general proportional to the temperature and therefore can be factored out. Thus, we can determine an estimate of the glass transition temperature by analyzing only the potential energy U_{pot} in the two systems, and the results are shown in Figure 10. Consistent with the density results, bulk and grafted systems are characterized by very similar potential energy plots and thus also by similar $T_g$values. By fitting the data at low and high temperatures with straight lines, we find again that T_g should be between 220 and 240 K for both systems, i.e., consistent with the value obtained from the density calculations.

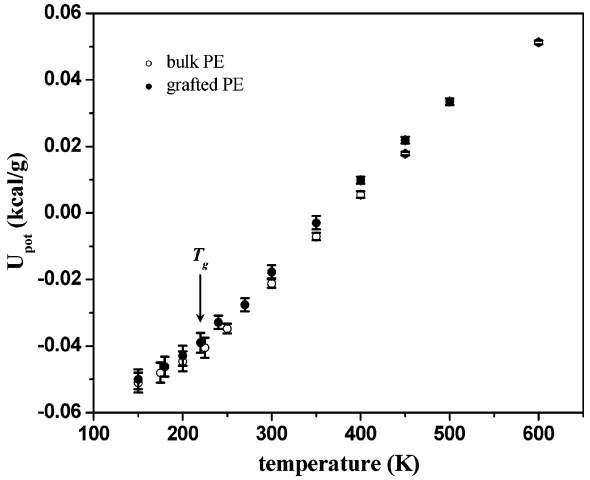

Figure 10. Effect of temperature T on the potential energy U_{pot} of the bulk (open circles) and grafted (filled circles) C_{156} PE system.

The simulation results for the dependence of the potential energy on temperature can be used to extract a prediction for the change Δc_p in the heat capacity c_p at the glass transition. Wunderlich[40] has reported a sharp rise in the heat capacity c_p of amorphous PE above 200 K. The point of inflection of the steep increase is the glass transition temperature (237 K), and the total change in c_p is equal to $\Delta c_p = 1.5 \times 10^{-4}$ kcal g^{-1} K^{-1}. Although the kinetic energy is not available in MC simulations, its contribution to the heat capacity can be calculated using the equipartition theorem and turns out to be 2.12×10^{-4} kcal g^{-1} K^{-1}. The jump in the heat capacity is due to the *configurational* contributions, which can be obtained from linear fits to the potential energy plots in the regions of low and high temperatures. The results obtained (the same for the two systems) are c_p^{conf} $(T < T_g) = (1.28 \pm 0.15) \times 10^{-4}$ kcal g^{-1} K^{-1} and c_p^{conf} $(T > T_g) = (2.48 \pm 0.10) \times 10^{-4}$ kcal g^{-1} K^{-1}. Based on this, we can then get an estimate for the change Δc_p in the specific heat at the glass transition. Our prediction is $(1.2 \pm 0.2) \times 10^{-4}$ kcal g^{-1} K^{-1}, which is close to the value of 1.5×10^{-4} kcal g^{-1} K^{-1} reported by Wunderlich. Due to the limited number of simulation data, the error bars accompanying them and the missing vibrational contributions in the MC data, an accurate calculation of c_p itself is not possible. However, we can report that the obtained values c_p $(T < T_g) = 3.4 \times 10^{-4}$ kcal g^{-1} K^{-1} and c_p $(T > T_g) = 4.6 \times 10^{-4}$ kcal g^{-1} K^{-1} are in reasonable agreement with the experimental data.[40]

Conclusions

We have shown that the EBMC method can be employed for simulations of a chemically realistic model of polyethylene in the neighborhood of its glass transition temperature. Both from volumetric as well as from enthalpic measurements, we obtain a glass transition temperature equal to $T_g = (230 \pm 10)$K. This is consistent with the values of T_g reported experimentally for amorphous polyethylene. The same T_g value was also obtained for a thin PE film with all of its chains grafted to a hard wall. These calculations validate the use of the novel EBMC technique down to the glass transition temperature. The data show that the autocorrelation function $f_{\mathbf{u}}(t)$ decays clearly to zero for temperatures around glass transition.

Of course, $f_{\mathbf{u}}(t)$ measures relaxation on the scale of the entire polymer chain which is mainly facilitated by the end-bridging moves. On the other hand, the other MC moves cause the system to relax at the local level. Relaxation at these more local length scales was confirmed by analyzing the time autocorrelation function of the Rouse modes along a PE chain. Although the almost perfect relaxation of the chain conformational properties that was observed at several temperatures just above the glass transition is surprising, we note that for the temperatures below T_g studied in this work, $f_{\mathbf{u}}(t)$ did not relax completely.

The study reported in this work shows the feasibility of using the EBMC simulation technique for determining the glass transition temperature of relatively long chains of polyethylene that are represented using a chemically realistic united-atom model. Thus, in a future work, the technique will be used to investigate the role played by the specific chemical interactions between the polymer and the substrate surface on the glass transition behavior of adsorbed films of polymers. The equilibrated model configurations accumulated in the course of the present EBMC simulations will also serve as starting points for executing long MD simulations with the same C_{156} PE system in order to estimate the temperature dependence of its Rouse relaxation spectrum and its frictional properties.[42]

Acknowledgment. O.A. and V.G.M. are grateful to the Greek Secretariat for Research and Technology (GSRT) for financial support in the course of this work through the PENED Greek National Programme, Code No O1EΔ 136. J.B. contributed to this work during a 3 month long student internship. He acknowledges support from the Department of Applied Physics of the Technical University of Eindhoven, The Netherlands. AB thanks support from the NSF (DMR 0517201). We thank Greg McKenna for many insightful discussions on the topic of glass transition behavior of polymer thin films. The authors are truly indebted to the anonymous reviewer for his/her suggestions and the very constructive comments during the reviewing process of the manuscript.

References and Notes

(1) Alcoutlabi, M.; McKenna, G. B. *J. Phys.: Condens. Matter* **2005**, *17*, R461.
(2) Forrest, J. A.; Dalnoki-Veress, K.; Stevens, J. R.; Dutcher, J. R. *Phys. Rev. Lett.* **1996**, *77*, 2002.
(3) Dalnoki-Veress, K.; Forrest, J. A.; Murray, C.; Gigault, C.; Dutcher, J. R. *Phys. Rev. E* **2001**, *63*, 031801.
(4) Forrest, J. A.; Dalnoki-Veress, K.; Dutcher, J. R. *Phys. Rev. E* **1997**, *56*, 5705.
(5) Wallace, W. E.; Van Zanten, J. H.; Wu, W. L. *Phys. Rev. E* **1995**, *52*, R3329.
(6) Sills, S.; Overney, R. M. *J. Chem. Phys.* **2004**, *120*, 5334.
(7) Priestley, R. D.; Ellison, C. J.; Broadbelt, L. J.; Torkelson, J. M. *Science* **2005**, *309*, 456.
(8) Tsui, O. K. C.; Russell, T. P.; Hawker, C. J. *Macromolecules* **2001**, *34*, 5535.
(9) Tate, R. S.; Fryer, D. S.; Pasqualini, S.; Montague, M. F.; de Pablo, J. J.; Nealey, P. F. *J. Chem. Phys.* **2001**, *115*, 9982.
(10) Baschnagel, J.; Varnik, F. J. *Phys.: Condens. Matter* **2005**, *17*, R851.
(11) Rigby, D.; Roe, R.-J. *J. Chem. Phys.* **1987**, *87*, 7285.
(12) Yang, L.; Srolovitz, D. J.; Yee, A. F. *J. Chem. Phys.* **1999**, *110*, 7058.
(13) Han, J.; Gee, R. H.; Boyd, R. H. *Macromolecules* **1994**, *27*, 7781.
(14) Varnik, F.; Baschnagel, J.; Binder, K. *Phys. Rev. E* **2002**, *65*, 021507.
(15) Peter, S.; Meyer, H.; Baschnagel, J. *J. Polym. Sci., Part B: Polym. Phys.* **2006**, *44*, 2951.
(16) Baljon, A. R. C.; Barber, DeGraaff, R.; v. Weert, M. H. M.; Khare, R. *Macromolecules* **2005**, *38*, 2391.
(17) Binder, K.; Paul, W. *J. Polym. Sci.,: Part B: Polym. Phys.* **1997**, *35*, 1.
(18) Mischler, C.; Baschnagel, J.; Binder, K. *Adv. Colloid Interface Sci.* **2001**, *94*, 197.
(19) Baschnagel, J.; Binder, K.; Wittmann, H.-P. *J. Phys.: Condens. Matter* **1993**, *5*, 1597.
(20) Jain, T. S.; de Pablo, J. J. *Macromolecules* **2002**, *35*, 2167.
(21) Pant, P. V. K.; Theodorou, D. N. *Macromolecules* **1995**, *28*, 7224.
(22) Mavrantzas, V. G.; Boone, T. D.; Zervopoulou, E.; Theodorou, D. N. *Macromolecules* **1999**, *32*, 5072.
(23) Doxastakis, M.; Mavrantzas, V. G.; Theodorou, D. N. *J. Chem. Phys.* **2001**, *115*, 11352.

(24) Gestoso, P.; Nicol, E.; Doxastakis, M.; Theodorou, D. N. *Macromolecules* **2003**, *36*, 6925.
(25) Daoulas, K. Ch.; Terzis, A. F.; Mavrantzas, V. G. *J. Chem. Phys.* **2002**, *116*, 11028.
(26) Daoulas, K. Ch.; Mavrantzas, V. G.; Photinos, D. J. *J. Chem. Phys.* **2003**, *118*, 1521.
(27) Daoulas, K. Ch.; Terzis, A. F.; Mavrantzas, V. G. *Macromolecules* **2003**, *36*, 6674.
(28) Mavrantzas, V. G.; Theodorou, D. N. *Macromolecules* **1998**, *31*, 6310.
(29) Mavrantzas, V. G.; Öttinger, H. C. *Macromolecules* **2002**, *35*, 960.
(30) Karayiannis, N. C.; Giannousaki, A. E.; Mavrantzas, V. G. *J. Chem. Phys.* **2003**, *118*, 2451.
(31) Van der Ploeg, P.; Berendsen, H. J. C. *J. Chem. Phys.* **1982**, *76*, 3271.
(32) Toxvaerd, S. *J. Chem. Phys.* **1997**, *107*, 5197.
(33) Martin, M. G.; Siepmann, J. I. *J. Phys. Chem. B* **1998**, *102*, 2569.
(34) Theodorou, D. N.; Suter, U. W. *Macromolecules* **1985**, *18*, 1467.
(35) Ciferri, A.; Hoeve, C. A. J.; Flory, P. J. *J. Amer. Chem. Soc.* **1961**, *83*, 1015.
(36) Auhl, R.; Everaers, R.; Grest, G. S.; Kremer, K.; Plimpton, S. J. *J. Chem. Phys.* **2003**, *119*, 12718.
(37) Ionescu, T.; Edwards, B. J.; Keffer, D.; Mavrantzas, V. G. 4th International workshop on nonequilibrium thermodynamics and complex fluids (IWNET 2006), Rhodes, Greece, September 3−7, 2006.
(38) Milner, S. T.; Witten, T. A.; Cates, M. E. *Macromolecules* **1988**, *21*, 2610.
(39) Milner, S. T.; Witten, T. A.; Cates, M. E. *Macromolecules* **1989**, *22*, 853.
(40) Wunderlich, B. *J. Chem. Phys.* **1962**, *37*, 1203.
(41) Loufakis, K.; Wunderlich, B. *J. Phys. Chem.* **1988**, *92*, 4205.
(42) Tsolou, G.; Mavrantzas, V. G. *J. Non-Newtonian Fluid Mech.* **2007**, http://dx.doi.org/10.1016/j.jnnfm.2007.10.011.

MA071173C